

Paper

Self-organization and spectral mechanism of attractor landscapes in high-capacity kernel Hopfield networks

Akira Tamamori  ¹¹ Aichi Institute of Technology, Aichi, 470-0392, Japan.

Received October 27, 20XX; Revised December 29, 20XX; Published July 1, 20XX

Abstract: Kernel-based learning methods can dramatically increase the storage capacity of Hopfield networks, yet the dynamical mechanisms behind this enhancement remain poorly understood. We address this gap by combining a geometric characterization of the attractor landscape with the spectral theory of kernel machines. Using a novel metric, *Pinnacle Sharpness*, we empirically uncover a rich phase diagram of attractor stability, identifying a *Ridge of Optimization* where the network achieves maximal robustness under high-load conditions. Phenomenologically, this ridge is characterized by a *Force Antagonism*, in which a strong driving force is counterbalanced by a collective feedback force. We theoretically interpret this behavior as a consequence of a specific reorganization of the weight spectrum, which we term *Spectral Concentration*. Unlike a simple rank-1 collapse, our analysis shows that the network on the ridge self-organizes into a critical regime: the leading eigenvalue is amplified to enhance global stability (Direct Force), while the trailing eigenvalues remain finite to sustain high memory capacity (Indirect Force). Together, these results suggest a spectral mechanism by which learning reconciles stability and capacity in high-dimensional associative memory models.

Key Words: Hopfield Network, Kernel Method, Dynamical System, Logistic Regression

1. Introduction

Associative memory, the ability to retrieve full patterns from partial or noisy cues, is a cornerstone of biological and artificial intelligence. The Hopfield network [1] provides a canonical model for this process, where memories are stored as stable fixed points (attractors) of an energy landscape. However, the classical model, governed by Hebbian learning, suffers from a severe storage limit ($P \approx 0.14N$) [2], restricting its practical utility.

Recent years have seen a resurgence of interest in high-capacity associative memories. Two dominant approaches have emerged. The first, exemplified by *Modern Hopfield Networks* (MHNs) and their connection to Transformers [3, 4], achieves capacity by redesigning the energy function itself (e.g., using exponential interaction terms) to sharpen the attractors. The second approach, which is the focus of this study, retains the standard quadratic energy structure (in a high-dimensional feature space) but employs sophisticated *learning algorithms* to optimize the synaptic weights. Our previous work demonstrated that Kernel Logistic Regression (KLR) learning falls into this category, achieving storage capacities ($P/N > 4.0$) comparable to MHNs while maintaining the simplicity of kernel dynamics [5].



Despite these performance gains, the underlying mechanism of KLR-trained networks remains a black box. Why does a discriminative learning rule (logistic regression) lead to a robust generative landscape? Unlike Gardner’s theory of capacity [6], which focuses on the volume of solution space, we lack a dynamical understanding of how the attractor geometry is sculpted. Specifically, the geometric properties that enable stability under such high loads are unknown.

This paper addresses this gap by unifying the *phenomenological* analysis of the attractor landscape with the *spectral* theory of kernel machines. We move beyond static capacity metrics to investigate the local geometry of stability.

Our contributions are threefold:

1. **Phenomenological Discovery:** Using a novel metric, “Pinnacle Sharpness,” we uncover a rich phase diagram of attractor stability. We identify a “Ridge of Optimization” where the network achieves maximal robustness. On this ridge, we observe a “Force Antagonism,” where a strong driving force is balanced by a collective feedback force.
2. **Theoretical Mechanism:** We propose a spectral theory to explain these observations. We establish a link between the geometric stability and the leading eigenvalue of the kernel Gram matrix. Based on this link, we reveal that the Ridge corresponds to a state of **Spectral Concentration**. Unlike a simple rank-1 collapse which would destroy memory capacity, our analysis shows that the network on the ridge self-organizes into a critical state: the leading eigenvalue is amplified to maximize global stability, while the trailing eigenvalues are preserved to maintain the rank required for multi-pattern storage.
3. **Unified Physical Picture:** We show that the observed Force Antagonism can be interpreted as a dynamical manifestation of Spectral Concentration. The dominant spectral mode creates a deep potential funnel (Direct Force), while the subordinate modes manage inter-pattern interference (Indirect Force).

By elucidating this spectral mechanism, we provide a principled explanation for the high performance of kernel associative memories, distinguishing our learning-based approach from energy-based designs like MHNs.

The remainder of this paper is organized as follows. Section 2 reviews related work, positioning our study within the context of capacity theory and kernel associative memories. Section 3 introduces the network model and defines the geometric metrics used for our analysis. Section 4 presents the phenomenological results, detailing the discovery of the Ridge and the associated Force Antagonism. Section 5 provides the theoretical core of this work, deriving the spectral mechanism of stability and validating the Spectral Concentration hypothesis. Finally, Section 6 discusses the broader implications of our findings, and Section 7 concludes the paper.

2. Related Work

The quest to enhance the storage capacity and robustness of associative memory has been a central theme in neural network research for decades. Our work sits at the intersection of dynamical systems, kernel methods, and modern dense associative memories.

2.1 From Classical to Modern Hopfield Networks

The classical Hopfield network [1], governed by the Hebbian learning rule, is theoretically elegant but practically limited by a storage capacity of $P \approx 0.14N$ [2]. To overcome this, researchers have proposed various modifications to the energy function. Polynomial interaction terms were introduced to increase capacity tensorially [7, 8]. More recently, Krotov and Hopfield proposed *Dense Associative Memories* using rectified polynomial energy functions, significantly boosting capacity [3]. Demircigil et al. further extended this to exponential energy functions, achieving exponential storage capacity [9]. A pivotal development was the work by Ramsauer et al., which established the equivalence between these exponential Hopfield networks and the attention mechanism in Transformers [4]. These Modern Hopfield Networks achieve high capacity by *designing* steep energy landscapes (e.g., Log-Sum-Exp). In contrast, our approach retains the standard quadratic energy structure (in the feature space) but leverages a powerful *learning algorithm* (KLR) to sculpt the landscape adaptively. This offers a complementary perspective: high capacity can arise from learning dynamics rather than just architectural definition.

2.2 Learning Algorithms and Capacity Theory

An alternative path to high capacity involves refining the learning rule. Gardner’s pioneering work established the theoretical capacity limit for patterns to be linearly separable [6]. The pseudo-inverse rule [10] and perceptron learning provide mechanisms to approach this limit by uncorrelating patterns.

The introduction of kernel methods brought non-linear separation capabilities to this domain. Early works extended associative memory models to feature spaces, incorporating kernel functions directly into the energy Hamiltonian [11] or utilizing kernelized pseudo-inverse rules [12]. Building on these foundations, recent approaches have applied discriminative learning, such as Support Vector Machines (SVMs) or Kernel Logistic Regression (KLR), to train recurrent networks by interpreting the dynamics as an iterative classification task. Our previous work established KLR as a highly effective rule for this purpose, achieving state-of-the-art capacity [5, 13].

However, these studies typically evaluate performance based on static classification metrics (e.g., margin) or final retrieval capacity. They rarely investigate the *dynamical mechanism*; specifically, it remains unclear how the learned weight spectrum shapes the global attractor landscape during the transient recall phase, which is the primary focus of this study.

2.3 Geometry and Spectrum of Neural Dynamics

Understanding the geometry of neural dynamics has been a longstanding goal, often approached through statistical mechanics [14] or information geometry [15]. Amari and Wu pioneered the geometric analysis of kernel machines, demonstrating how a kernel function induces a Riemannian metric in the input space that governs the spatial resolution of classification [15]. Our work complements these theoretical foundations by introducing a data-driven spectral perspective. While statistical mechanics often assumes the thermodynamic limit ($N \rightarrow \infty$) with random patterns, and classical information geometry focuses on static classifiers, our spectral analysis of the Ridge and Spectral Concentration provides a concrete mechanism for the dynamics of finite-size networks. It explains how the system self-organizes its weight spectrum to balance stability (via the leading eigenvalue) and diversity (via the trailing eigenvalues), offering a bridge between abstract geometric theories and the actual stability of learned attractors.

3. Model and Methods

We consider a standard Hopfield network architecture trained using Kernel Logistic Regression (KLR). In this section, we first define the network model and the learning algorithm. We then introduce our primary analytical tools: a geometric indicator for phenomenological analysis and a spectral framework for theoretical interpretation.

3.1 Kernel Logistic Regression Hopfield Network

We consider a network of N bipolar neurons, $s \in \{-1, 1\}^N$, trained to store P patterns $\{\xi^\mu\}_{\mu=1}^P$. The KLR learning rule determines the dual variables $\alpha_{\mu i}$ for each neuron i by minimizing a regularized logistic loss. The network state s evolves synchronously based on the input potential:

$$h_i(s) = \sum_{\mu=1}^P \alpha_{\mu i} K(s, \xi^\mu) \quad (1)$$

$$s_i(t+1) = \text{sign}(h_i(s(t))), \quad (2)$$

where $K(\cdot, \cdot)$ is the RBF kernel with width parameter γ .

3.2 Phenomenological Tool: Pinnacle Sharpness and Force Decomposition

To quantitatively analyze the stability of the attractors, we investigate the geometry of the network’s energy landscape. While the synchronous KLR dynamics do not guarantee the monotonic decrease of a traditional energy function, we define a Lyapunov function candidate whose landscape reflects the restorative forces of the system:

$$V(s) := - \sum_{k=1}^N s_k h_k(s), \quad (3)$$

where $h_k(s)$ is the input potential defined in Eq. (2). This function measures the alignment between the current state s and the input field.

We utilize the ‘‘Pinnacle Sharpness’’, defined as the squared norm of the gradient of this function at a stored pattern:

$$M(\xi^\mu) := \|\nabla V(s)\|^2|_{s=\xi^\mu}. \quad (4)$$

To calculate the gradient, we treat the discrete state s as a continuous variable $\mathbf{x} \in \mathbb{R}^N$. This continuous relaxation is introduced solely as a local surrogate to probe the stability geometry in the neighborhood of discrete fixed points, rather than as an exact description of the underlying dynamics. Differentiating Eq. (3) yields the gradient vector, which we analytically decompose into two functionally distinct components:

$$\nabla V(\mathbf{x}) = \mathbf{F}_d(\mathbf{x}) + \mathbf{F}_i(\mathbf{x}). \quad (5)$$

The first component, the **Direct Force** \mathbf{F}_d , is defined as:

$$\mathbf{F}_d(\mathbf{x}) := -\mathbf{h}(\mathbf{x}). \quad (6)$$

This term represents the immediate drive for the state vector to align with its own input field. The second component, the **Indirect Force** \mathbf{F}_i , captures the collective feedback effects and is given by:

$$[\mathbf{F}_i(\mathbf{x})]_j = -\sum_{k=1}^N x_k \frac{\partial h_k(\mathbf{x})}{\partial x_j}. \quad (7)$$

This term describes how a change in neuron j perturbs the inputs to all other neurons k , and how those perturbations reflexively influence the energy. We measure the alignment between these two forces using their cosine similarity $\rho(s)$.

3.3 Theoretical Framework: Spectral Representation

To provide a mathematical basis for the observed forces and stability, we introduce a spectral representation of the network dynamics.

Matrix Representation of Weights: While kernel Hopfield networks do not store an explicit $N \times N$ weight matrix, the effective linear operator \mathbf{W} in the high-dimensional feature space \mathcal{H} governs the dynamics. Crucially, this operator is finite-rank and can be fully characterized by the stored patterns and the learned dual variables. Let $\phi : \mathbb{R}^N \rightarrow \mathcal{H}$ be the feature mapping associated with the RBF kernel, which maps the input state into a high-dimensional Reproducing Kernel Hilbert Space (RKHS) \mathcal{H} . Let $\Phi = [\phi(\xi^1), \dots, \phi(\xi^P)]$ be the feature matrix collecting the mapped patterns. The weight operator can be written as:

$$\mathbf{W} = \Phi \alpha \Phi^\top, \quad (8)$$

where $\alpha \in \mathbb{R}^{P \times P}$ is the matrix of learned dual coefficients.

The Kernel Gram Matrix: The geometry of the patterns in the feature space is encoded in the kernel Gram matrix $\mathbf{K} \in \mathbb{R}^{P \times P}$, with entries $K_{\mu\nu} = K(\xi^\mu, \xi^\nu) = \langle \phi(\xi^\mu), \phi(\xi^\nu) \rangle$.

Spectral Connection: A key insight of our theoretical approach is that the stability of the dynamical system (the Hessian of the energy) is spectrally equivalent to the product of the dual coefficients and the Gram matrix. Specifically, the eigenvalues governing the basin depth and shape are determined by the spectrum of $\alpha^{1/2} \mathbf{K} \alpha^{1/2}$ (assuming positive definite α). This formulation allows us to translate the physical ‘‘sharpness’’ of attractors directly into the ‘‘spectral gap’’ of the kernel matrix, providing a bridge between the learning algorithm (which optimizes α) and the resulting physics of the memory landscape.

Information Geometric Framework: To analyze the learning dynamics, we also employ tools from Information Geometry. The KLR model forms a statistical manifold equipped with the Fisher Information Matrix (FIM) as a Riemannian metric. For a single neuron, the FIM \mathbf{G} is given by $\mathbf{G} = \mathbf{K} \mathbf{D} \mathbf{K}$, where \mathbf{D} is a diagonal matrix of prediction variances. This metric allows us to distinguish between the Euclidean Gradient ∇L , which guides standard SGD, and the Natural Gradient $\tilde{\nabla} L = \mathbf{G}^{-1} \nabla L$, which represents the steepest descent direction on the manifold. The interplay between these two gradients reveals the intrinsic geometry of the learning process. A detailed derivation of these concepts is provided in Appendix B.

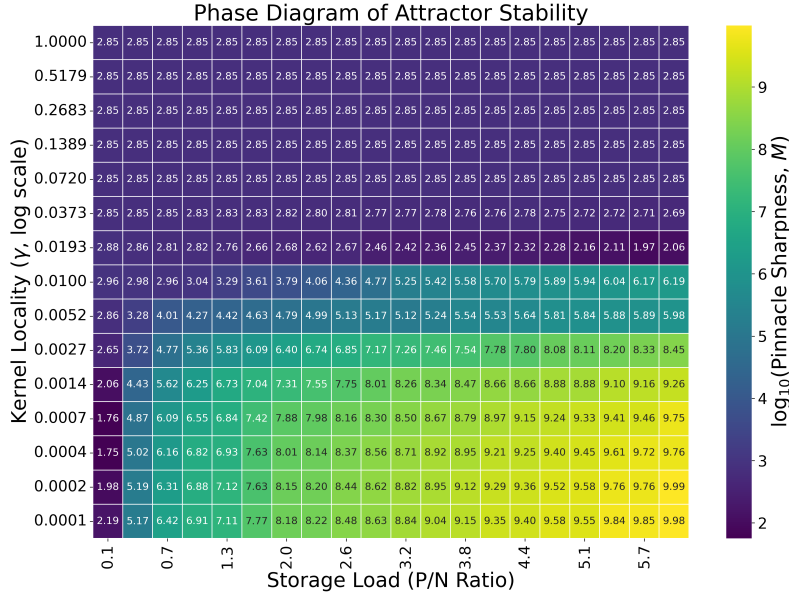


Figure 1. Phase diagram of attractor stability, quantified by the Pinnacle Sharpness M . The heatmap shows $\log_{10} M$ as a function of kernel locality γ and storage load P/N . Three regimes are visible: (i) a local regime (large γ), (ii) a global, inefficient regime (small γ , low load), and (iii) a remarkable **Ridge of Optimization** (bright diagonal band) where the network achieves maximal stability. This ridge corresponds to the spectral “Goldilocks zone” identified in our theoretical analysis.

4. Phenomenology: Discovery of the Optimization Ridge

Our previous study established that KLR-trained networks achieve exceptional storage capacity and noise robustness [5]. Building on this performance baseline, this section presents the results of large-scale numerical simulations designed to uncover the dynamical mechanism governing this stability.

We first demonstrate that the local stability of attractors, quantified by our Pinnacle Sharpness metric, exhibits a complex dependency on network parameters, revealing a rich phase structure. We then dissect the underlying mechanism by analyzing the interplay between the constituent forces of the landscape gradient.

4.1 The Phase Diagram of Attractor Stability

To obtain a global view of how attractor stability is organized, we systematically computed the Pinnacle Sharpness, M , across a wide range of the kernel locality parameter γ and the storage load P/N . For each pair of $(\gamma, P/N)$, a KLR Hopfield network with $N = 100$ neurons was trained using the optimization protocol detailed in [5]. The Pinnacle Sharpness was then calculated at the center of a randomly chosen stored pattern ξ^μ .

The results are summarized in the phase diagram shown in Figure 1. This figure plots the \log_{10} of the Pinnacle Sharpness as a heatmap. The diagram reveals a strikingly complex and organized structure, which can be characterized by three distinct regions:

1. **The Local, Non-Cooperative Regime:** In the upper region of the diagram, corresponding to large gamma values ($\gamma > 0.05$), the Pinnacle Sharpness remains largely constant at a moderate level, irrespective of the storage load P/N . In this regime, the kernel’s influence is highly localized, suggesting that each attractor is stabilized independently without significant interaction from other stored patterns.
2. **The Global, Inefficient Regime:** In the lower-left region, where γ is small and P/N is low, the Pinnacle Sharpness drops to its lowest values. Here, the kernel is global, but the scarcity of patterns provides insufficient information for the learning algorithm to form sharp, well-defined attractors. The energy landscape is consequently flat and lacks strong restorative forces.
3. **The Ridge of Optimization:** The most remarkable feature of the phase diagram is the emergence of a “ridge” of extremely high Pinnacle Sharpness, extending diagonally from the lower-left to the lower-right. Along this ridge, the network achieves a level of attractor stability that is orders of magnitude greater

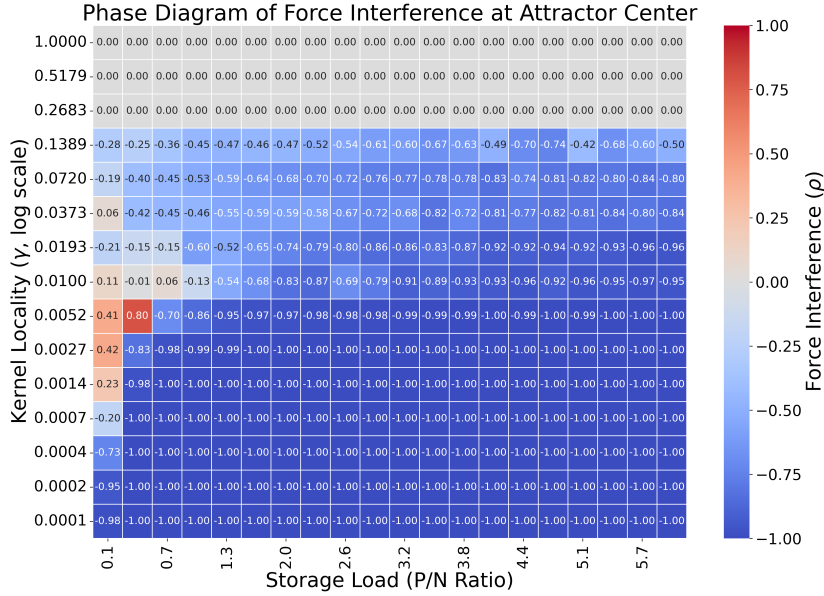


Figure 2. Phase diagram of Force Interference ρ , measuring the cosine similarity between the Direct Force F_d and Indirect Force F_i . Blue regions indicate strong anti-correlation (antagonism, $\rho \approx -1$). The Ridge of Optimization in Fig. 1 precisely traces the transition boundary into this antagonistic regime, suggesting that stability is maintained by a delicate balance of opposing spectral forces.

than in the other regimes. This indicates that, faced with the dual challenges of a global kernel (small γ) and high memory congestion (large P/N), the network does not simply fail. Instead, it enters a highly optimized state, suggesting a sophisticated self-organization mechanism is at play.

4.2 Decomposing the Forces: The Mechanism of Self-Organization

To understand the origin of the Ridge, we analyzed the behavior of the two constituent forces of the landscape gradient: the direct force F_d and the indirect feedback force F_i . We computed the normalized correlation between these two forces, the Force Interference $\rho(x)$, across the same parameter space.

The resulting phase diagram is shown in Figure 2. This figure reveals a clear transition. In the local regime (large γ), the interference is approximately zero, confirming that the two forces act largely independently. However, as gamma decreases, the interference rapidly transitions to a state of strong anti-correlation ($\rho \approx -1$). This indicates that in the global regime, the indirect feedback force F_i actively opposes the direct force F_d .

This strong anti-correlation provides the key to understanding the ridge. The Pinnacle Sharpness, $\|\nabla V\|^2$, is given by $\|F_d\|^2 + \|F_i\|^2 + 2\langle F_d, F_i \rangle$. When $\rho \approx -1$, this simplifies to $\|\nabla V\|^2 \approx (\|F_d\| - \|F_i\|)^2$. This means that the Pinnacle Sharpness is determined by the difference in the magnitudes of the two opposing forces.

4.3 The Nature of the Optimization Ridge

Finally, to elucidate the nature of the Ridge, we analyzed the magnitudes of the individual forces along a representative cross-section of the phase diagram. We fixed gamma to a small value ($\gamma = 0.001$), where the cooperative anti-correlation is strong, and plotted the log-magnitudes of $\|F_d\|^2$, $\|F_i\|^2$, and the resulting Pinnacle Sharpness ($\|\nabla V\|^2$) as a function of the storage load P/N .

The result is shown in Figure 3. This plot clearly reveals the mechanism behind the optimization ridge. As P/N increases, both $\|F_d\|^2$ (blue line) and $\|F_i\|^2$ (green line) increase by orders of magnitude. However, the direct force F_d grows at a substantially faster rate than the indirect force F_i . Because the two forces are in strong opposition ($\rho \approx -1$), the total Pinnacle Sharpness (red line) is determined by their difference, $(\|F_d\| - \|F_i\|)^2$, and is therefore dominated by the explosive growth of the direct force.

This leads to our final conclusion. The Ridge of Optimization is a regime where: (1) the direct and indirect forces are in a state of strong, cooperative anti-correlation, and (2) the learning algorithm, driven by the high storage load, amplifies the magnitude of the direct force F_d to a level that vastly overwhelms the opposing feedback force F_i . The resulting large net force creates the exceptionally sharp and stable attractors observed.

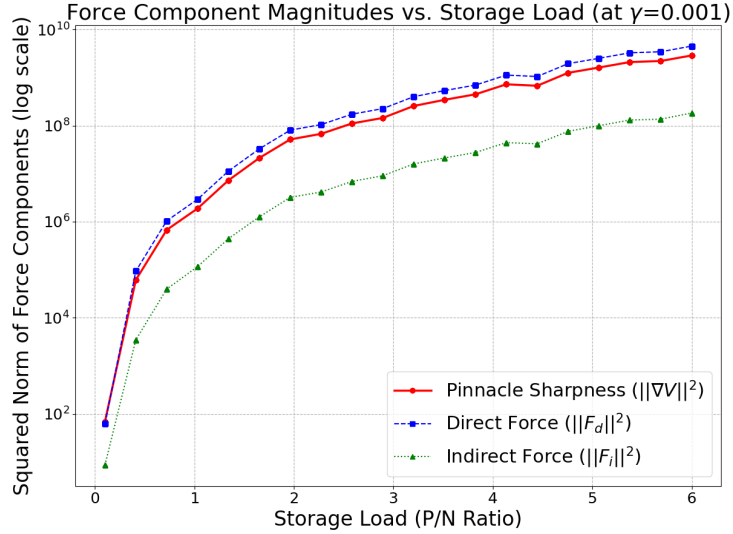


Figure 3. Growth of force component magnitudes as a function of storage load P/N for a fixed small γ . The Direct Force (blue, $\|F_d\|^2$) grows significantly faster than the Indirect Force (green, $\|F_i\|^2$). Theoretically, this reflects the amplification of the leading spectral mode (λ_1) due to Spectral Concentration, which allows the driving force to overwhelm the interference and create a deep attractor basin.

This is a remarkable demonstration of a system achieving extreme stability not through the synergy of forces, but through a controlled and amplified antagonism.

5. Theoretical Analysis: Spectral Mechanism of Self-Organization

This section provides a theoretical interpretation of the phenomenology reported in Section 4.

The phenomenological experiments in Section 4 presented a compelling puzzle: the emergence of the Ridge where stability is maximized amidst strong Force Antagonism. In this section, we solve this puzzle. We posit that these phenomena are manifestations of a spectral phase transition in the learned network. We first deduce this mechanism theoretically and then validate it with targeted experiments.

5.1 Theory: Spectral Mechanism of Stability

To provide a theoretical explanation for the observed Ridge and the associated Force Antagonism, we analyze the spectral properties of the network in the feature space. We propose a two-step mechanism: first, we link the geometric stability to the spectral properties of the kernel, and second, we characterize the unique spectral state that emerges on the Ridge.

5.1.1 Step 1: The Geometry-Spectrum Link

The local stability of an attractor is geometrically quantified by the Pinnacle Sharpness M . Although the dynamics are defined by the kernel update rule, the underlying curvature of the energy landscape is governed by the Hessian matrix. By analyzing the Hessian in the reproducing kernel Hilbert space (see Appendix A.2 for derivation), we establish a direct link between the attractor’s geometry and the spectrum of the learned model.

Proposition 1 (Stability-Spectrum Link). *The Pinnacle Sharpness $M(\xi^\mu)$ scales proportionally with the largest eigenvalue λ_{\max} of the effective Gram matrix $\mathbf{K}_\alpha = \alpha^{1/2} \mathbf{K} \alpha^{1/2}$:*

$$M(\xi^\mu) \propto \lambda_{\max}(\mathbf{K}_\alpha), \quad (9)$$

where the proportionality holds up to kernel-dependent constants under the local isometry approximation.

This proposition provides the fundamental principle: to maximize attractor stability (and thus noise robustness), the learning algorithm must find a configuration of dual variables α that maximizes the dominant spectral mode of the system.

5.1.2 Step 2: Spectral Concentration on the Ridge

Based on Proposition 1, we can now interpret the Ridge. We hypothesize that the high stability observed in this regime is not due to a uniform strengthening of all weights, but rather due to a specific reorganization of the spectral structure. We term this phenomenon **Spectral Concentration**.

Proposition 2 (Spectral Concentration, empirical and heuristic). *On the Ridge of Optimization, the matrix α exhibits strong spectral concentration. The leading eigenvalue becomes dominant ($\lambda_1 \gg \lambda_k$ for $k > 1$), thereby maximizing the Pinnacle Sharpness via Proposition 1. Crucially, unlike a rank-1 collapse, the trailing eigenvalues remain non-zero ($\lambda_k > 0$), maintaining the full-rank structure necessary to store multiple patterns.*

Appendix A.3 provides a theoretical justification for this phenomenon. It explains how the maximum-margin objective naturally leads to a spectral structure that amplifies the principal mode for stability while preserving separability for capacity.

This spectral structure explains the dual nature of the network’s high performance:

1. **Global Stability:** The massive leading eigenvalue λ_1 creates a steep, deep potential funnel (Direct Force) that strongly pulls states towards the stored patterns.
2. **Memory Capacity:** The non-zero trailing eigenvalues preserve the fine-grained information required to distinguish between different patterns, preventing them from collapsing into a single spurious attractor.

The Force Antagonism observed in Section 4 is the dynamical signature of this spectral hierarchy: the dominant mode exerts the primary restorative force, while the subordinate modes manage the interference to ensure separability.

5.2 Empirical Validation of the Theory

To confirm that Spectral Concentration is indeed the mechanism behind the Ridge, we analyzed the spectral properties of the learned dual variables $\alpha \in \mathbb{R}^{P \times P}$.

Effective Rank Analysis: We utilized the *Stable Rank* (numerical rank) to quantify the spectral distribution of α . For singular values $\sigma_1 \geq \sigma_2 \geq \dots \geq \sigma_P \geq 0$, the Stable Rank is defined as:

$$\text{StableRank}(\alpha) := \frac{\sum_{i=1}^P \sigma_i^2}{\sigma_1^2}. \quad (10)$$

A lower Stable Rank indicates a more concentrated spectrum, where the leading mode dominates the energy. As shown in Fig. 4, the region where the Stable Rank is minimal perfectly overlaps with the Ridge observed in Fig. 1. Note that while the rank is significantly reduced compared to the random initialization, it does not collapse to exactly 1.0, consistent with the requirement for multi-pattern storage.

Eigenvalue Spectrum: We further examined the detailed eigenvalue distribution of α at specific points. Fig. 5 reveals a striking contrast that explains the mechanism:

- **Off Ridge (Global):** The spectrum (green dotted line) shows a sharp collapse, resembling a rank-1 structure. This corresponds to the low-capacity regime where memories merge into a single attractor.
- **Off Ridge (Local):** The spectrum (blue dashed line) is flat and diffuse, indicating that the network fails to establish a dominant stability mode.
- **On the Ridge:** The spectrum (red solid line) exhibits a unique **intermediate structure**. It features a distinct leading mode (σ_1) that drives stability, yet crucially maintains a slowly decaying, heavy tail ($\sigma_{k>1}$). This confirms that the Ridge represents a Goldilocks zone where the network maximizes stability via spectral concentration without suffering from rank collapse.

These results provide direct empirical evidence that the Ridge corresponds to a phase where the network self-organizes into a state of extreme spectral concentration.

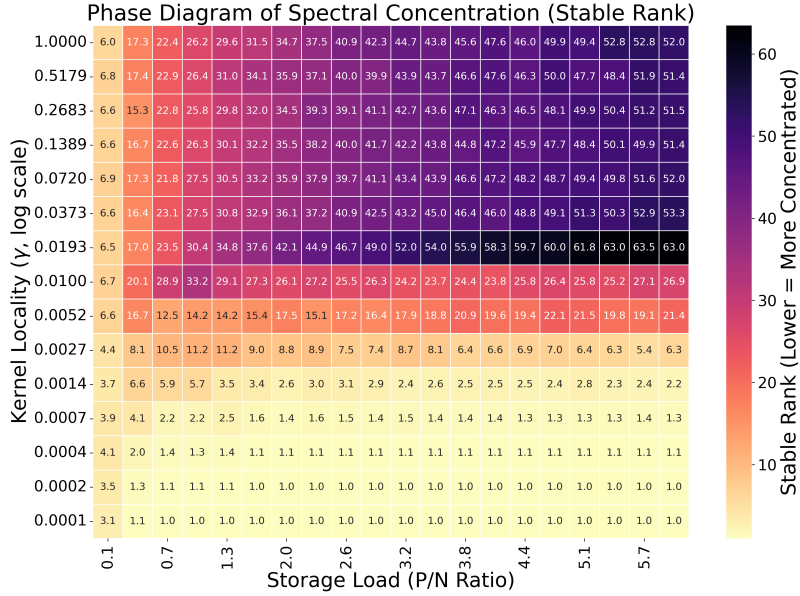


Figure 4. Heatmap of the Stable Rank (effective rank) of the dual variable matrix α across the phase diagram. Lower values (lighter/yellow colors) indicate a more concentrated spectrum. Crucially, the region of minimal Stable Rank perfectly aligns with the Ridge of Optimization observed in Fig. 1, confirming that maximal attractor stability is achieved when the weight spectrum becomes highly concentrated (but not fully collapsed to rank 1).

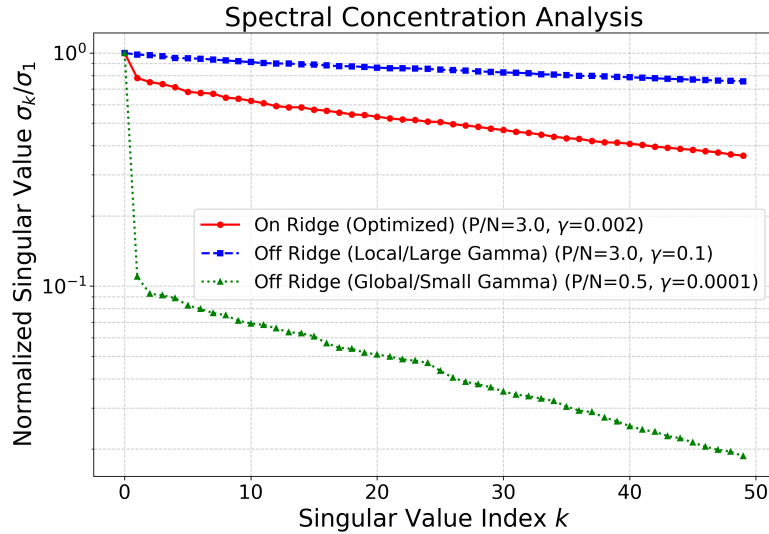


Figure 5. Comparison of eigenvalue spectra of the dual variable matrix α at three characteristic points in the phase diagram. **Green (Global/Low Load):** The spectrum exhibits a sharp rank-1 collapse ($\lambda_1 \gg \lambda_2 \approx 0$), leading to memory loss. **Blue (Local/High Gamma):** The spectrum is diffuse ($\lambda_k \approx \text{const}$), resulting in weak stability. **Red (On Ridge):** The spectrum shows **Spectral Concentration**, characterized by a dominant leading eigenvalue for stability (λ_1) coexisting with a non-zero heavy tail ($\lambda_{k>1}$) for capacity. This “L-shaped” structure confirms the theoretical prediction of a critical balance.

5.3 Unified Interpretation

The combination of phenomenological observation (Force Antagonism) and spectral evidence (Spectral Concentration) leads to a unified physical picture. The Ridge represents a sweet spot where the kernel locality γ is tuned such that the system can amplify the principal spectral mode to form deep, sharp attractors (via Proposition 1), while effectively managing inter-pattern interference using the remaining spectral degrees of freedom. The Force Antagonism can be interpreted as the dynamical manifestation of this spectral disparity:

the massive Direct Force arises from the dominant λ_1 component, while the Indirect Force reflects the collective contribution of the trailing modes, acting to refine the basin boundaries.

6. Discussion

In this work, we have moved beyond simple performance metrics to provide a clear physical picture of the self-organization mechanism in KLR-trained Hopfield networks. Our central finding is the discovery of a Ridge of Optimization and its spectral origin, Spectral Concentration. Here, we discuss the broader implications of these findings.

6.1 The Ridge as a Critical Phase Boundary

The spectral analysis in Fig. 5 revealed that the Ridge represents a critical state. The network does not simply maximize the leading eigenvalue to the point of rank-1 collapse, which would imply a trivial memory with unit capacity. Instead, it maintains a delicate balance: maximizing λ_1 for global stability while preserving a non-zero tail ($\lambda_{k>1}$) for pattern discriminability. This suggests that the Ridge can be interpreted as a **phase boundary** or a Goldilocks zone between an ordered phase (rank-1, low capacity) and a disordered phase (diffuse spectrum, weak stability). This observation aligns with the hypothesis of *Self-Organized Criticality* in biological neural networks [16], where systems tune themselves to a critical point to maximize information processing capabilities.

It is important to distinguish Spectral Concentration from simple dimensionality reduction techniques like Principal Component Analysis (PCA). PCA blindly discards trailing eigenvalues to minimize reconstruction error, often leading to the loss of pattern identity (similar to rank-1 collapse). In contrast, KLR learning is discriminative; it actively preserves the “heavy tail” of the spectrum exactly to the extent required to maintain the decision boundaries between patterns. Thus, the Ridge represents an optimal compression that balances energy minimization (via the leading mode) with classification margin (via the trailing modes).

6.2 The Information Geometry of Learning

Our spectral theory explains the static properties of the Ridge, but how the learning dynamics navigate to this critical state remains an open question. Here, we provide an *information-geometric interpretation* of the empirically observed learning dynamics, which suggests that the Ridge acts as a **geometric barrier** at the brink of singularity. As shown in Fig. B-1, the learning dynamics at the edge of the Ridge ($\gamma = 0.01$) exhibit a pronounced divergence in the norm of the Natural Gradient. This behavior is consistent with an effective pinning of the learning trajectory near the boundary of the manifold.

Importantly, the approach to this regime is not chaotic but highly structured. As illustrated in Fig. B-2, the dynamics on the stable part of the Ridge ($\gamma = 0.02$) display a two-phase learning process: an initial phase dominated by the acquisition of global stability, followed by a prolonged fine-tuning phase that refines memory capacity. From an information-geometric viewpoint, this behavior can be interpreted as learning guided by an emergent curved geometry. Consistent with this interpretation, the learning trajectory traces a distinct parabolic arc in parameter space (Fig. B-3), which is characteristic of gradient flow on a curved statistical manifold.

6.3 Comparison with Modern Hopfield Networks

Recent advances in associative memory, such as Modern Hopfield Networks (MHNs) [3, 4], achieve high capacity by modifying the energy function to include steep non-linearities (e.g., exponential or polynomial terms). In contrast, our approach demonstrates that similar high-performance regimes can be accessed within the standard quadratic energy framework (in feature space), provided the weights are learned via a discriminative objective like KLR. This is significant because quadratic energy models are often more amenable to implementation on neuromorphic hardware and analytical tractability. Our results show that the *learning rule* can be just as powerful as the *architecture design* in determining the memory landscape.

6.4 Practical Implications and Future Directions

The clean, spurious-free landscape achieved by Spectral Concentration makes KLR Hopfield networks an attractive candidate for reliable content-addressable memory systems. However, the computational cost of kernel evaluations scales with the number of stored patterns. Future work should explore sparse approximations

(e.g., Nyström method [17] or Random Fourier Features [18]) to reduce the effective rank explicitly, potentially enforcing the “Spectral Concentration” structure by design to achieve linear scaling. Furthermore, extending this spectral theory to analyze the dynamics of Transformer attention layers, which share mathematical similarities with kernel memories, remains an exciting avenue for research.

Furthermore, our discovery of Spectral Concentration provides a theoretical justification for using low-rank approximations in kernel machines. The fact that the effective weight matrix naturally exhibits a low stable rank on the Ridge implies that sparse approximation methods, such as the Nyström method, can capture the essential dynamics without significant loss of performance, paving the way for scalable implementations.

7. Conclusion

In this paper, we have presented a coherent theoretical account of attractor self-organization in high-capacity kernel Hopfield networks. Moving beyond conventional performance metrics, we investigated the dynamical and spectral mechanisms that allow these networks to operate near classical storage limits.

Our phenomenological analysis identified a Ridge of Optimization in the phase diagram, where the network achieves maximal stability and exhibits a distinctive Force Antagonism. We theoretically interpreted this behavior through its spectral origin, which we termed **Spectral Concentration**. On the Ridge, learning drives the weight spectrum toward a critical regime in which the leading eigenvalue is amplified to enhance global stability, while the remaining eigenvalues remain finite, enabling high-capacity storage. This picture goes beyond a simple rank-1 collapse and instead characterizes the optimal memory landscape as a finely balanced interplay between attractive forces and pattern discriminability.

By linking the geometry of attractors with the spectral structure of the kernel machine, this work provides a principled framework for understanding how learning induces self-organized memory states. More broadly, the notion of spectral concentration offers insight into how stability and capacity can be reconciled in associative systems, and may inform the analysis of related learning dynamics in modern kernel- and attention-based architectures.

Funding

Not applicable.

Conflicts of interest

The authors declare no competing interests.

Author contribution

All the authors contributed equally to the present work.

Artificial intelligence tools

We used ChatGPT (GPT-5.2) and Gemini 2.5 Pro for proofreading the English manuscript.

Appendix

A. Spectral Theory of Kernel Attractors

This appendix provides the theoretical derivations linking the attractor stability to the spectral properties of the kernel Gram matrix, supporting the propositions in Section 5.

A.1 Notation and Setup

Let \mathcal{H} be the reproducing kernels Hilbert space associated with the kernel $K(\mathbf{x}, \mathbf{y})$. The stored patterns are mapped to feature vectors $\phi(\xi^\mu) \in \mathcal{H}$. We define the feature matrix $\Phi = [\phi(\xi^1), \dots, \phi(\xi^P)]$ and the Gram matrix $K = \Phi^\top \Phi \in \mathbb{R}^{P \times P}$. The weight operator W in \mathcal{H} is represented as $W = \Phi \alpha \Phi^\top$, where $\alpha \in \mathbb{R}^{P \times P}$ are the learned dual coefficients.

A.2 Proof of Proposition 1 (Stability-Spectrum Link)

We aim to show that the Hessian of the energy function, which governs the local stability in the input space, is spectrally related to the kernel Gram matrix in the feature space.

The energy function is defined as $E(s) = -\frac{1}{2}\langle\phi(s), \mathbf{W}\phi(s)\rangle$. Let s^* be a fixed point. The Hessian matrix $H = \nabla^2 E(s^*)$ is dominated by the first-order term (Gauss-Newton approximation):

$$H \approx J^\top \mathbf{W} J, \quad (\text{A-1})$$

where we define the sign convention such that H represents the magnitude of the curvature (positive definite around a stable attractor), ignoring the negative sign from the energy definition. J is the Jacobian matrix of the feature map $\phi(s)$ at s^* .

To analyze the spectrum of H , consider the quadratic form with respect to an arbitrary unit vector \mathbf{u} in the input space ($\|\mathbf{u}\|^2 = 1$):

$$\mathbf{u}^\top H \mathbf{u} = \mathbf{u}^\top (J^\top \mathbf{W} J) \mathbf{u} = (J\mathbf{u})^\top \mathbf{W} (J\mathbf{u}). \quad (\text{A-2})$$

Let $\mathbf{v} = J\mathbf{u}$ be the mapped vector in the feature space. A key property of the RBF kernel is its local isometry; the mapping scales local distances uniformly. Specifically, using the Taylor expansion of the kernel, one can show that the squared norm scales as $\|\mathbf{v}\|^2 = \mathbf{u}^\top (J^\top J) \mathbf{u} \approx 2\gamma \|\mathbf{u}\|^2 = 2\gamma$.

Thus, maximizing the curvature $\mathbf{u}^\top H \mathbf{u}$ in the input space is equivalent to maximizing the quadratic form $\mathbf{v}^\top \mathbf{W} \mathbf{v}$ in the feature space, subject to the norm constraint on \mathbf{v} . Substituting the weight operator $\mathbf{W} = \Phi \alpha \Phi^\top$, the relevant spectral properties are determined by the non-zero eigenvalues of the matrix product $\Phi^\top \mathbf{W} \Phi$ (restricted to the span of patterns), which reduces to analyzing the effective Gram matrix:

$$\mathbf{K}_\alpha = \alpha^{1/2} \mathbf{K} \alpha^{1/2}. \quad (\text{A-3})$$

Note that the non-zero eigenvalues of \mathbf{K}_α are identical to those of $\alpha \mathbf{K}$. Consequently, the Pinnacle Sharpness $M(\xi^\mu)$, which corresponds to the squared gradient norm (and scales with the dominant curvature), is proportional to the leading eigenvalue of this matrix:

$$M \propto \lambda_{\max}(\mathbf{K}_\alpha). \quad (\text{A-4})$$

This confirms Proposition 1.

A.3 Theoretical Basis for Spectral Concentration (Proposition 2)

Here we provide a heuristic justification for why the optimization leads to Spectral Concentration on the Ridge.

In the high-load or high-regularization regime, Kernel Logistic Regression approximates a maximum-margin objective in the feature space. The dual optimization problem involves maximizing a quadratic form $\alpha^\top \mathbf{K} \alpha$ subject to constraints. Let \mathbf{v}_1 be the eigenvector of the Gram matrix \mathbf{K} associated with the largest eigenvalue λ_1 . If there is a spectral gap ($\lambda_1 > \lambda_2$), the direction \mathbf{v}_1 offers the most efficient way to increase the margin (or stability).

Consequently, the optimization algorithm is biased to align the weight vector α primarily with \mathbf{v}_1 to maximize the objective. This creates a large disparity in the spectrum of α , where the component along \mathbf{v}_1 is amplified:

$$\frac{\mathbf{v}_1^\top \alpha \mathbf{v}_1}{\mathbf{v}_k^\top \alpha \mathbf{v}_k} \gg 1 \quad \text{for } k > 1. \quad (\text{A-5})$$

However, unlike a pure rank-1 collapse, the constraints of storing P distinct patterns require that α retains non-zero components along other directions ($\mathbf{v}_{k>1}$) to ensure linear separability of all patterns. This balance results in the observed Spectral Concentration: a dominant λ_1 for stability, coexisting with a non-zero tail for capacity.

B. Information Geometric Formulation

This appendix provides a brief overview of the information geometric concepts used in Section 6 to analyze the learning dynamics. We follow the standard formulation by Amari [19].

B.1 Statistical Manifold and Fisher Metric

The set of probability distributions defined by the KLR model forms a statistical manifold M . Each point on this manifold corresponds to a specific set of parameters α , which in information geometry are known as the *natural parameters* (or θ -coordinates). The distance between two nearby points on this manifold, corresponding to parameters α and $\alpha + d\alpha$, is measured by the infinitesimal change in the probability distribution. This distance is quantified by the Fisher Information Matrix (FIM) $G(\alpha)$, which acts as a Riemannian metric tensor.

For a single neuron, the probability of the output being +1 is given by the sigmoid of the logit $u = \sum_u \alpha_u K(\cdot, \xi^\mu)$. This follows a Bernoulli distribution, which is a member of the exponential family. For such models, the FIM is defined as the expectation of the outer product of the gradient of the log-likelihood:

$$G_{\mu\nu}(\alpha) = \mathbb{E} \left[\frac{\partial \log p}{\partial \alpha_\mu} \frac{\partial \log p}{\partial \alpha_\nu} \right]. \quad (\text{B-1})$$

A key property of the logistic function is that $\partial p / \partial \alpha_\mu = (y - p)K(\cdot, \xi^\mu)$, where y is the target and p is the model's output probability. Taking the expectation over the data distribution (and assuming independence), this leads to the specific form used in the main text:

$$G = KDK, \quad (\text{B-2})$$

where D is a diagonal matrix with entries $D_{\mu\mu} = p_\mu(1 - p_\mu)$ representing the prediction variance for pattern ξ^μ .

B.2 Natural Gradient Descent

Standard gradient descent (SGD) follows the steepest descent direction in the Euclidean parameter space. However, this path is not necessarily the steepest on the curved statistical manifold. The direction of steepest descent on the manifold is given by the *Natural Gradient* [20].

The Natural Gradient $\tilde{\nabla}L$ is defined as the direction that maximizes the decrease in the loss function L for a small, fixed ‘‘information distance’’ (measured by the KL-divergence). For an infinitesimal step, the KL-divergence between $p(\alpha)$ and $p(\alpha + d\alpha)$ is approximated by the quadratic form of the Fisher metric:

$$D_{\text{KL}}(p(\alpha) || p(\alpha + d\alpha)) \approx \frac{1}{2} d\alpha^\top G(\alpha) d\alpha. \quad (\text{B-3})$$

Minimizing the change in loss $\nabla L^\top d\alpha$ subject to a fixed information distance leads to the Natural Gradient direction:

$$\tilde{\nabla}L(\alpha) = G(\alpha)^{-1} \nabla L(\alpha). \quad (\text{B-4})$$

The Natural Gradient Descent (NGD) update rule is therefore $\alpha_{t+1} = \alpha_t - \eta \tilde{\nabla}L(\alpha_t)$. This formulation allows us to analyze the learning dynamics not as a simple descent in Euclidean space, but as a flow on a curved Riemannian manifold, revealing the geometric distortions induced by the FIM.

B.3 Experimental Analysis of Learning Dynamics

To validate the geometric interpretations presented in the Discussion, we conducted numerical analyses of the SGD learning trajectory. We tracked the parameter vector α_t for a single representative neuron over 200 training steps under different hyperparameter regimes.

Gradient Norm Dynamics: We computed the squared norms of three distinct gradient vectors at each step t : the Euclidean norm $\|\nabla L(\alpha_t)\|^2$, the Riemannian norm $\|\nabla L(\alpha_t)\|_{G^{-1}}^2 = \nabla L^\top G^{-1} \nabla L$, and the Natural Step norm $\|G^{-1} \nabla L(\alpha_t)\|^2$. As shown in Fig. B-1, the dynamics on the edge of the Ridge ($\gamma = 0.01$) exhibit a divergence in the Riemannian and Natural Step norms. This indicates that the manifold is approaching a singularity, creating a geometric barrier for SGD.

Pythagorean Decomposition of Information Gain: Second, we decomposed the information gain at each step, $\Delta I_t \approx \frac{1}{2} \delta_t^\top G^* \delta_t$ into two orthogonal components based on the eigenspace of the final FIM G^* : the Principal Gain (contribution from λ_1 and the Tail Gain (contribution from $\lambda_{k>1}$). As shown in Fig. B-2, the dynamics on the stable part of the Ridge ($\gamma = 0.02$) exhibit a two-phase process: an initial phase dominated

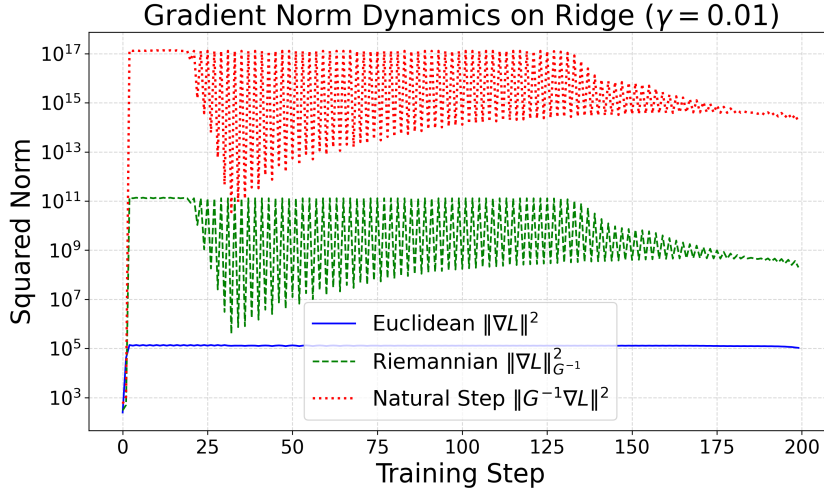


Figure B-1. Gradient Norm Dynamics on the Edge of the Ridge ($\gamma = 0.01$). The divergence of the Riemannian and Natural Step norms indicates that the manifold is approaching a singularity, creating a geometric barrier for SGD.

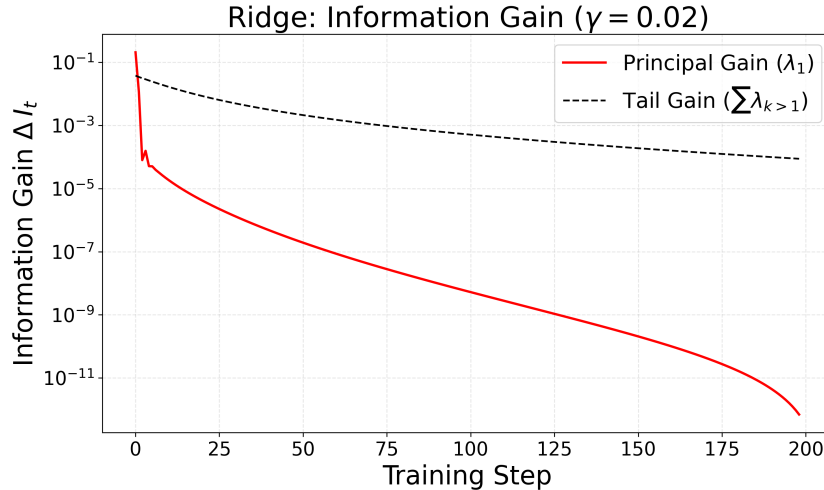


Figure B-2. Information Gain Decomposition on the Ridge ($\gamma = 0.02$). The dynamics exhibit a two-phase process: an initial phase dominated by Principal Gain is followed by a prolonged Fine-tuning phase dominated by Tail Gain.

by Principal Gain is followed by a prolonged Fine-tuning phase dominated by Tail Gain, demonstrating a hierarchical learning strategy.

Geodesic Deviation: Finally, we analyzed the shape of the trajectory α_t by plotting its deviation from the e-geodesic (straight line) against its progress towards the final state α^* . As shown in Fig. B-3, the results reveal a stark contrast between the two regimes: while the Local trajectory ($\gamma = 0.1$) is perfectly straight, the Ridge trajectory ($\gamma = 0.02$) forms a distinct parabolic arc. This confirms that the trajectory on the Ridge is guided by the non-trivial curvature of the statistical manifold.

References

- [1] J.J. Hopfield, “Neural networks and physical systems with emergent collective computational abilities,” Proceedings of the National Academy of Sciences, vol.79, no.8, pp.2554–2558, 1982.
- [2] D.J. Amit, H. Gutfreund, and H. Sompolinsky, “Storing infinite numbers of patterns in a spin-glass model of neural networks,” Phys. Rev. Lett., vol.55, pp.1530–1533, Sep 1985.
- [3] D. Krotov and J.J. Hopfield, “Dense associative memory for pattern recognition,” Proceedings of the 30th International Conference on Neural Information Processing Systems, NIPS’16, Red Hook, NY, USA, p.1180–1188, Curran Associates Inc., 2016.

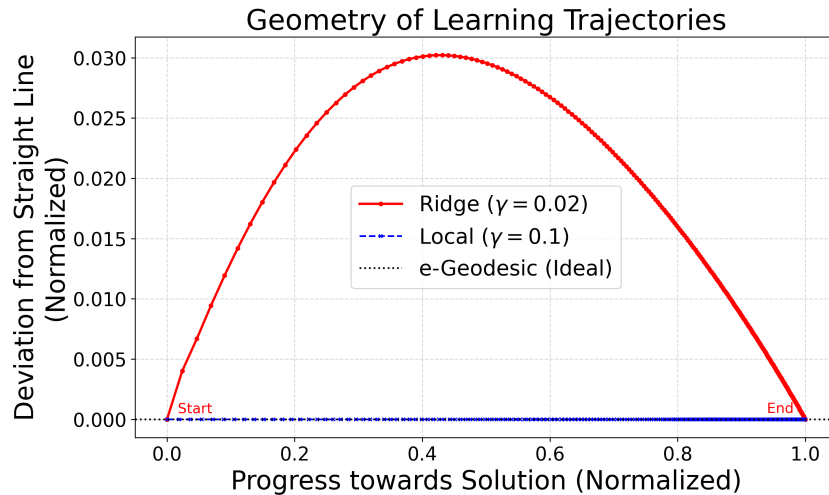


Figure B-3. Geodesic Deviation of Learning Trajectories. The Ridge trajectory ($\gamma = 0.02$, red solid line) exhibits a distinct parabolic arc, demonstrating that it is guided by the non-trivial curvature of the statistical manifold. In stark contrast, the Local trajectory ($\gamma = 0.1$, blue dashed line) follows the e-geodesic (straight line) perfectly, indicating a flat, featureless learning landscape.

- [4] H. Ramsauer, B. Schäfl, J. Lehner, P. Seidl, M. Widrich, T. Adler, L. Gruber, M. Holzleitner, M. Pavlović, G.K. Sandve, V. Greiff, D. Kreil, M. Kopp, G. Klambauer, J. Brandstetter, and S. Hochreiter, “Hopfield networks is all you need,” arXiv preprint arXiv:2008.02217, 2021.
- [5] A. Tamamori, “Quantitative attractor analysis of high-capacity kernel hopfield networks,” arXiv preprint arXiv:2505.01218, 2025.
- [6] E. Gardner, “The space of interactions in neural network models,” *Journal of Physics A: Mathematical and General*, vol.21, no.1, p.257, jan 1988.
- [7] H.H. Chen, Y.C. Lee, G.Z. Sun, H.Y. Lee, T. Maxwell, and C.L. Giles, “High order correlation model for associative memory,” *AIP Conference Proceedings*, vol.151, no.1, pp.86–99, 08 1986.
- [8] D. Psaltis, and C.H. Park, “Nonlinear discriminant functions and associative memories,” *AIP Conference Proceedings*, vol.151, no.1, pp.370–375, 1986.
- [9] M. Demircigil, J. Heusel, M. Löwe, S. Uppgang, and F. Vermet, “On a model of associative memory with huge storage capacity,” *Journal of Statistical Physics*, vol.168, pp.288–299, 2017.
- [10] L. Personnaz, I. Guyon, and G. Dreyfus, “Collective computational properties of neural networks: New learning mechanisms,” *Phys. Rev. A*, vol.34, pp.4217–4228, Nov 1986.
- [11] B. Caputo and H. Niemann, “Storage capacity of kernel associative memories,” *Proceedings of the International Conference on Artificial Neural Networks, ICANN '02, Berlin, Heidelberg*, p.51–56, Springer-Verlag, 2002.
- [12] D. Nowicki and H. Siegelmann, “Flexible kernel memory,” *PLOS ONE*, vol.5, no.6, pp.1–18, 06 2010.
- [13] A. Tamamori, “Kernel logistic regression learning for high-capacity hopfield networks,” *IEICE Transactions on Information and Systems*, vol.E109-E, no.2, 2026.
- [14] A.C. Coolen, *The mathematical theory of minority games: statistical mechanics of interacting agents*, Oxford University Press, 2005.
- [15] S. Amari and S. Wu, “Improving support vector machine classifiers by modifying kernel functions,” *Neural Networks*, vol.12, no.6, pp.783–789, 1999.
- [16] J.M. Beggs and P. Dietmar, “Neuronal avalanches in neocortical circuits,” *Journal of Neuroscience*, vol.23, no.35, pp.11167–11177, Society for Neuroscience, 2003.
- [17] C.K.I. Williams and M. Seeger, “Using the nyström method to speed up kernel machines,” *Advances in Neural Information Processing Systems*, 2000.
- [18] A. Rahimi and B. Recht, “Random features for large-scale kernel machines,” *Advances in Neural Information Processing Systems*, ed. J. Platt, D. Koller, Y. Singer, and S. Roweis, Curran Associates, Inc., 2007.

- [19] S. Amari, "Information geometry and its applications," vol.194, Springer, 2016.
- [20] S. Amari, "Natural gradient works efficiently in learning," Neural Computation, vol.10, no.2, pp.251–276, 1998.